Sustainable Valorization of Salak Peel Waste: Regeneration of Biochar for Lead Removal from Wastewater

Phruektinai Buakhiao, Thatchapol Chungcharoen*, Aud Jamkamon, Warunee Limmun, and Dithaporn Thungsotanon

Department of Engineering, King Mongkut's Institute of Technology Ladkrabang, Prince of Chumphon Campus, Chumphon, 86160, Thailand

Email: phuttinai.prompt@gmail.com (P.B.); thatchapol.ch@kmitl.ac.th (T.C.); jamkamonaud@gmail.com (A.J.); warunee.li@kmitl.ac.th (W.L.); Dithaporn.th@kmitl.ac.th (D.T.)

*Corresponding author

Manuscript received September 22, 2025; revised October 14, 2025; accepted November 19, 2025; published March 18, 2026

***Abstract*—This study evaluates the effects of pyrolysis temperature (600 °C and 800 °C, denoted as SP600 and SP800) and regeneration reagents on lead (Pb^{2+}) adsorption performance of biochar derived from salak peels. Moreover, the lead removal efficiency and adsorption efficiency after several regeneration cycles under appropriate conditions were also investigated. The results indicate that increasing the pyrolysis temperature significantly enhances lead removal efficiency and adsorption capacity, with biochar pyrolyzed at 800 °C and loaded with lead (SP800Pb) exhibiting the highest initial lead adsorption performance. However, upon regeneration using hydrochloric acid (HCl) and sodium nitrate ($NaNO_3$) at various concentrations, SP600Pb demonstrated higher lead removal performance than SP800Pb across all conditions. Specifically, SP600Pb regenerated by 0.1 M HCl exhibited the highest lead desorption efficiency and removal efficiency. Furthermore, after five consecutive adsorption-regeneration cycles, the biochar regenerated by 0.1 M HCl (SP600RPb) exhibited a suitable removal efficiency of 83.91±0.10% and a desorption efficiency of 148.73±0.13%. The observed desorption efficiency exceeding 100% was attributed to the accumulated release of Pb^{2+} ions during successive regeneration cycles, which indicates enhanced ion-exchange dynamics over time. Therefore, biochar pyrolyzed at 600 °C and regenerated using 0.1 M HCl is appropriate for the reuse of biochar in lead adsorption, promoting sustainable resource application, cost reduction, and waste minimization in production processes.**

***Keywords*—biomass, salak peels, biochar regeneration, lead adsorption, Sustainable Development Goals (SDGs), circular economy, ecological adsorbent**

I. Introduction

Currently, environmental problems caused by anthropogenic waste are continuously increasing. Specifically, large quantities of organic and inorganic pollutants have been released into terrestrial and aquatic ecosystems, primarily from the industrial and agricultural sectors. These contaminants significantly degrade the quality of natural resources, affecting both human health and ecological systems [1]. Among these pollutants, heavy metals such as lead (Pb^{2+}) pose serious threats due to their non-biodegradable nature, ultimately endangering environmental sustainability and human health [2]. Consequently, effective waste management is of paramount importance. One promising strategy is to leverage specific types of waste, particularly agricultural waste, to produce value-added products. This approach reduces waste accumulation and enhances the sustainability of resource applications.

Agricultural waste constitutes the largest share of global waste, accounting for 80% of the total waste from various sectors [3]. In this context, salak peel waste from salak fruit processing industries is abundant in Chumphon, Thailand. Furthermore, the chemical composition of salak peel, which contains high levels of cellulose (~47 wt%) and lignin (~22.3 wt%), demonstrates promising potential as a precursor material for high-quality biochar production [4]. Biochar is a products derived from biomass conversion via pyrolysis, a thermal decomposition process under oxygen-limited conditions. Pyrolysis temperature is a key factor influencing the physical and chemical properties of the resulting biochar, including functional groups, specific surface area, pore size, and pore distribution [5]. Biochars produced below 600 °C often result in incomplete carbonization, leading to a structure that retains a high amount of volatile matter and exhibits poor thermal stability. In contrast, elevated temperatures exceeding 800 °C promote the excessive decomposition of oxygen-containing functional groups and can lead to the collapse of microstructural features essential for maintaining chemical reactivity [6]. Therefore, identifying the appropriate pyrolysis temperature is critical for producing high-quality biochar. Due to its favorable characteristics, biochar has been widely applied for various purposes, including fuel combustion, soil amendment, and wastewater treatment, especially for the adsorption of heavy metals such as Pb^{2+} [7]. Compared with other adsorbent materials such as activated carbon, biochar offers a more sustainable and cost-effective alternative due to its low production cost, simple preparation, and reduced environmental footprint [8]. Its utilization promotes waste valorization and supports the circular economy by converting agricultural residues into useful materials. This approach directly contributes to the United Nations Sustainable Development Goals (SDGs), highlighting the importance of clean water, responsible resource management, and sustainable production practices [9, 10]. Moreover, adsorption using regenerable biochar represents a more sustainable and cost-effective alternative to coagulation- flocculation, which generates large amounts of chemical sludge [11]. However, one of the key challenges in biochar application is the significant decline in adsorption efficiency after several cycles, which often leads to higher production costs due to the need for continuous replacement of spent biochars [12]. Therefore, regeneration is essential to restore the adsorption efficiency of spent biochar to levels comparable to the first use. This approach reduces production costs and adds value to agricultural waste by promoting its sustainable reuse.

Regeneration is a critical process used to remove contaminants from the surface of the spent biochar, allowing the material to be reused and reducing production costs. Among the available techniques, chemical regeneration with hydrochloric acid (HCl) and sodium nitrate ($NaNO_3$) has been demonstrated to be an effective method for restoring biochar functionality. HCl functions by releasing hydrogen ions (H^+) to displace lead ions (Pb^{2+}) adsorbed on the biochar surface, while $NaNO_3$ serves as an ion-exchange agent without causing significant structural changes to the biochar, thereby helping to restore its lead adsorption efficiency [13]. However, the concentration of these chemical regenerants directly influences both the regeneration efficiency and the physicochemical structure of biochar, which are critical factors requiring thorough investigation to determine the appropriate concentration conditions for application.

The objective of this research is to investigate the influence of pyrolysis temperature and regeneration reagents (type and concentration) on the lead removal efficiency and adsorption capacity of biochar derived from salak peel. Furthermore, the lead removal and adsorption efficiencies after several regeneration cycles under appropriate conditions are also examined. This approach contributes to adding value to agricultural waste and promoting sustainable environmental management.

II. Literature Review

Heavy metal contamination, particularly from lead (Pb^{2+}), represents a global environmental challenge. As a toxic, non-biodegradable element, lead pollution presents serious risks to human health and ecosystems. The primary sources of lead contamination are industrial and agricultural activities. Consequently, the development of effective strategies for lead remediation is of critical importance. Among these strategies, biochar derived from agricultural wastes has emerged as a promising adsorbent for heavy metal removal in wastewater, primarily due to its low production cost, large specific surface area, highly porous structure, and functional groups.

From 2009 to 2016, research primarily focused on the effects of pyrolysis temperature (100–700 °C) and biomass type, such as agricultural residues, wood chips, food scraps, and industrial organic waste, on the heavy metal adsorption capacity of various metals, including lead (Pb^{2+}), copper (Cu^{2+}), zinc (Zn^{2+}), and cadmium (Cd^{2+}), as well as associated adsorption mechanisms. The findings demonstrated that biomass rich in cellulose and hemicellulose, combined with appropriate pyrolysis conditions, enhances adsorption capacity via mechanisms such as ion exchange, electrostatic attraction, precipitation, and physical sorption [14–17]. However, challenges remain regarding reuse performance. Biochar tends to lose adsorption capacity over repeated cycles, mainly due to pore blockage and surface degradation.

From 2017 to 2024, research has shifted to focus on strategies for biochar regeneration for reuse. Acidic and alkaline solutions, including H_2SO_4, HCl, NaOH, and $NaNO_3$, were investigated for this purpose [18–24]. Among the various chemical regenerants, HCl and $NaNO_3$ are widely regarded as the most effective due to their desorption efficiency and minimal structural impact on biochar. HCl releases hydrogen ions (H^+) that effectively displace metal ions adsorbed on active sites through ion exchange, while its moderate acidity prevents the excessive degradation of surface functional groups, which is often caused by stronger acids such as sulfuric acid (H_2SO_4) [23]. In contrast, $NaNO_3$ serves as a neutral salt regenerant that promotes ion exchange without altering the surface chemistry or pore morphology of biochar [24]. Compared with alkaline solutions such as NaOH, which can dissolve mineral constituents and damage the carbon matrix, $NaNO_3$ preserves the material's structural integrity during successive regeneration cycles. However, detailed investigations into the effects of HCl and $NaNO_3$ concentrations on lead adsorption and desorption remain limited. Additionally, studies on the regeneration capacity of these solutions with respect to adsorption capacity are still deficient. Therefore, identifying appropriate regeneration conditions is key to improving the practical applicability of biochar in future wastewater treatment systems.

III. Materials and Methods

A. Materials and Chemicals

The Salak Peels (SPs) used for biochar production were obtained from a fruit processing industry in Chumphon, Thailand. The SPs were first washed with Deionized (DI) water, sieved to a particle size of less than 425 μm, and then dried at 105 °C until a constant weight was achieved. Lead(II) nitrate ($Pb(NO_3)_2$) and sodium nitrate ($NaNO_3$) were purchased from Merck, USA.

B. Biochar Preparation

The SPs were subjected to pyrolysis at 600 °C and 800 °C in a reactor. Nitrogen (N_2) flowed through the tube at 200 mL/min throughout the pyrolysis process. The heating rate was 5 °C/min up to the target temperature of 600 °C and 800 °C. The maximum temperature was maintained for 1 h then cooled to mbient temperature. The resulting biochar was repeatedly rinsed with DI water until the wash solution reached a neutral pH (pH 7 or close to 7) and was subsequently stored in a drying oven at 105 °C until use. The biochars produced at 600 °C and 800 °C were named SP600 and SP800, respectively. The biochar yields produced at various temperatures were measured and determined according to Eq. (1):

$$\text{Biochar yields (wt\%)} = \frac{W_b}{W_{sp}} \times 100\% \quad (1)$$

where W_{sp} and W_b (g) are the initial weight of the salak peels and the final weight of the biochar, respectively.

C. Biochar Characterization

Analysis of the biochar's characteristics, including specific surface area, pore volume, and pore diameter, was performed by nitrogen (N_2) adsorption-desorption using a Brunauer–Emmett–Teller (BET) method (TriStar II 3020, Micromeritics, USA). Surface morphologies of the samples were observed using Field-Emission Scanning Electron Microscopy and Energy Dispersive Spectroscopy (FESEM-EDS) (Thermo Fisher Scientific Co., Ltd., USA). Chemical functional groups were measured by Fourier Transform Infrared Spectroscopy (FT-IR) (Perkin-Elmer, USA) in the range of 400–4000 cm^{-1}. The electrical conductivity of the biochar was observed using a resistivity chamber (Keithley Model 6150) (Tektronix Co., Ltd.,

USA). The elemental content of the biochar was determined using an elemental analyzer (Flash Smart CHNS/O, Thermo Fisher Scientific Co., Ltd., USA).

D. Experimental of Pb^{2+} adsorption

Lead (Pb^{2+}) adsorption onto SP600 and SP800 was evaluated using batch adsorption. Precisely 0.02 g of each biochar was added to separate 50 mL centrifuge tubes, followed by the addition of 20 mL of Pb^{2+} solution at an initial concentration (C_0) of 30 mg/L. The samples were shaken at 200 rpm under isothermal conditions at 30 °C for 24 h to ensure equilibrium adsorption. After adsorption, the suspensions were filtered using nylon membrane filters (0.25 μm pore size, GE cellulose nylon membrane) to separate the biochar from the Pb^{2+} solution. The filtrates were subsequently collected and analyzed for Pb^{2+} concentration using Inductively Coupled Plasma Optical Emission Spectrometry (ICP-OES) (AVIO 500, PerkinElmer, USA). The removal efficiency and adsorption capacity were calculated as follows:

$$\text{Removal efficiency (\%)} = \frac{C_0\text{-}C}{C_0} \times 100\% \quad (2)$$

$$\text{Adsorption capacity (mg/g)} = \frac{(C_0\text{-}C)\times V_{sol}}{M_{abs}} \quad (3)$$

where C_0 and C (mg/L) are the initial and equilibrium concentration of Pb^{2+}, respectively; V_{sol} (L) and M_{abs} (g) are the volume of the solution and the mass of biochar used, respectively.

E. Biochar Regeneration

The regeneration of spent biochar was performed to restore its Pb^{2+} adsorption capacity. Hydrochloric acid (HCl) and sodium nitrate ($NaNO_3$) solutions at concentrations of 0.1, 0.05, and 0.01 M were prepared as regeneration reagents. The spent biochar samples obtained after Pb^{2+} adsorption were introduced into 50 mL centrifuge tubes. Subsequently, 20 mL of the regenerating solution was added to each tube. The mixtures were shaken at 200 rpm under isothermal conditions at 30 °C for 3 h. After desorption, the suspensions were filtered using nylon membrane filters (0.25 μm pore size, GE cellulose nylon membrane) to separate the biochar from the regenerating solution. The filtrates were subsequently collected and analyzed for Pb^{2+} concentration using ICP-OES. The desorption efficiency was calculated according to Eq. (4):

$$\text{Desorption efficiency (\%)} = \frac{C_R}{C_0\text{-}C} \times 100\% \quad (4)$$

where C_R (mg/L) is the equilibrium concentration of Pb^{2+} in the regeneration solution, C_0 and C (mg/L) are the initial and equilibrium concentration of Pb^{2+} from the preceding adsorption step, respectively.

After regeneration, the biochar was washed with DI water until a Neutral pH (pH 7) was reached, then dried at 105 °C for 24 h. The regenerated biochar was subsequently reused in up to five successive Pb^{2+} adsorption cycles to evaluate its reusability and stability.

F. Economic Evaluation

The adsorption cost and cost per cycle were calculated to evaluate the overall cost-effectiveness of the biochar, integrating economic feasibility with actual adsorption performance. The adsorption cost and cost per cycle were calculated as follows:

$$\text{Adsorbent cost (THB/g)} = \frac{\text{Total production cost}}{\text{Biochar yield}} \quad (5)$$

$$\text{Cost per cycle (THB/cycle)} = \frac{\text{Total production cost}}{\text{Number of cycles}} \quad (6)$$

IV. Result and Discussion

A. Biochar Characterization

The physicochemical properties of the biochars are presented in Table 1. Biochar yields varied significantly with pyrolysis temperature: SP600 exhibited the highest average yield, while SP800 produced the lowest. This decrease corresponds with an increase in Carbon (C) content observed in SP800, accompanied by decreases in hydrogen (H) and Oxygen (O) contents. These changes reflect the enhanced thermal degradation of the major organic components in biomass, including cellulose, hemicellulose, and lignin [25].

The Specific Surface Area (S_{BET}) of the biochar increased significantly from 6.274 m^2/g in SP600 to 8.783 m^2/g in SP800. This indicates a transition towards a more developed porous structure, which plays an important role in enhancing the adsorption capacity for small molecules, supporting applications such as contaminant removal [26]. The total pore volume (V_{total}) also increased from 0.011 cm^3/g in SP600 to 0.030 cm^3/g in SP800. This increase corresponds to the improved porosity promoted by higher pyrolysis temperature, primarily attributed to the opening of previously blocked pores caused by the decomposition of organic matter [25]. The average pore sizes of SP600 and SP800 were 1.188 nm and 1.185 nm, respectively, both falling within the microporous range. This similarity suggests that changes in pyrolysis temperature had little influence on the average pore size, with the primary impact being on the number and distribution of pores.

The ultimate elemental composition was examined to understand the influence of chemical constituents on lead adsorption. The C content significantly increased from 65.80 wt% in SP600 to 73.66 wt% in SP800, indicating improved structural stability at higher pyrolysis temperatures. This enhancement is primarily attributed to the greater removal of non-carbon elements, such as Hydrogen (H), Nitrogen (N), and Oxygen (O), during high-temperature pyrolysis. The Oxygen (O) content notably decreased from 19.95 wt% in SP600 to 12.35 wt% in SP800, mainly due to its release as carbon monoxide (CO), carbon dioxide (CO_2), and other volatile matters. Similarly, reductions in hydrogen (H) and nitrogen (N) contents were observed, indicating the decomposition of organic functional groups containing these elements [27]. Conversely, the ash content exhibited a slight increase with rising pyrolysis temperature. This increase resulted from the accumulation of thermally stable inorganic residues remaining after the decomposition of organic matter [28].

Elemental ratios, including O/C, H/C, and (O+N)/C, were employed to evaluate the chemical structure of the biochars. The O/C ratio decreased from 0.303 in SP600 to 0.168 in SP800, indicating the removal of oxygen-containing

functional groups as the pyrolysis temperature increased. This reduction corresponds to the formation of a more stable carbon structure, consistent with the observed decline in oxygen (O) content. Similarly, the H/C ratio declined from 0.022 to 0.011, suggesting an increased degree of aromaticity, which contributes to enhanced structural integrity and resistance to microbial degradation [29]. The reduction in the (O+N)/C ratio from 0.317 to 0.178 further indicates a decrease in polar functional groups, which may influence the adsorption properties of the biochars.

The pH of the biochar increases with rising pyrolysis temperature as shown in Table 1 (pH 9.78 for SP600 and pH 10.6 for SP800). This results from the decomposition of organic compounds within the SP structure at elevated temperatures. As the temperature increases, acidic and neutral organic constituents are removed as gases and bio-oil, leaving a carbon-rich residue. This residue typically exhibits higher purity and is often associated with increased alkalinity due to the concentration of basic inorganic mineral oxides [30].

Table 1. Physicochemical properties of the biochars obtained under different temperatures

Biochars	Yields (%)	Ultimate analysis (wt%)					Ash (wt%)	Atomic ratio			S_{BET} (m^2/g)	V_{total} (cm^3/g)	Pore diameter (nm)	pH
		C	H	N	O	S		H/C	O/C	(O+N)/C				
SP600	32.55±0.12	65.80	1.45	0.87	19.95	ND*	11.93	0.022	0.303	0.317	6.274	0.011	1.188	9.78
SP800	31.30±0.05	73.66	0.77	0.76	12.35	ND*	12.46	0.011	0.168	0.178	8.783	0.030	1.185	10.6

S_{BET} (m^2/g) is the Brunauer-Emmett-Teller (BET) surface area.
V_{total} (cm^3/g) is the total volume in Pores.
ND* means not detected (DL = 0.01% S).

Table 2. Lead adsorption performance of biochar at different temperatures

Sample	Adsorption capacity (mg/g)	Removal efficiency (%)	Electrical conductivity (S/cm)
SP600	29.84 ± 0.09^{a}	99.47 ± 0.09^{a}	$(5.52\pm0.39)\times10^{-6a}$
SP800	29.95 ± 0.07^{b}	99.84 ± 0.05^{b}	$(9.71\pm0.94)\times10^{-5b}$

Note: $^{a-b}$Means with different superscripts are significantly different ($p < 0.05$).

Additionally, Electrical Conductivity (EC) was analyzed (Table 2) to evaluate the biochar's potential for heavy metal adsorption. The EC of biochar increased significantly as the pyrolysis temperature rose from 600 to 800 °C, with SP600 and SP800 showing values of $(5.52\pm0.39) \times 10^{-6}$ S/cm and $(9.71\pm0.94) \times 10^{-5}$ S/cm, respectively. This increase was primarily due to the enhanced carbonization and graphitization processes at higher temperatures, which led to a greater proportion of sp^2-hybridized carbon within the carbon matrix. Meanwhile, the content of heteroatoms (H, O, N) decreased, reducing structural distortion in the carbon network and allowing for more continuous electron pathways [31]. This increasingly ordered carbon framework facilitates electron transport primarily via an electron hopping mechanism between interconnected sp^2 domains, which plays a key role in the EC enhancement. Furthermore, higher temperatures also promoted the migration of metal minerals, including Fe, Ca, and Mg, to the biochar surface, leading to the formation of conductive percolation networks and reducing internal contact resistance within the carbon matrix [32]. These findings are consistent with those reported by Bardiet *et al.* [33], indicating that the EC increased as the pyrolysis temperature rose from 400 to 700 °C, mainly due to decreases in H/C and O/C ratios and increased aromatization of the biomass structure.

FT-IR spectra (Fig. 1) were employed to examine the effect of pyrolysis temperature on the surface functional groups. A broad absorption band corresponding to hydroxyl (-OH) groups was observed at 3770 cm^{-1}. The intensity of this band decreased in SP800, indicating the decomposition of functional groups during high-temperature pyrolysis [34]. Alkane (C-H) stretching vibrations were observed between 2960–2820 cm^{-1}, with slightly greater intensity in SP600, suggesting a reduction in aliphatic chains as pyrolysis temperature increased. The alkyne (C≡C) groups observed at 2180 cm^{-1} suggest the formation of triple-bonded carbon structures due to structural rearrangements at high pyrolysis temperatures [35]. An absorption band at 1750 cm^{-1} indicated the presence of carbonyl (C=O) stretching, attributed to carboxylic acids or ketones, which exhibited higher intensity in SP600, consistent with its higher Oxygen content (O). Aromatic (C=C) stretching vibrations were detected at 1520 cm^{-1} for both SP600 and SP800, with greater intensity in SP800, reflecting the development of aromatic structures at elevated temperatures [36]. Oxygen-containing functional groups, such as alcohols (C-O) stretching at 1160 cm^{-1} and esters (C-O-C) stretching at 1025 cm^{-1}, exhibited higher intensity in SP600, further confirming the decomposition of oxygen-containing linkages at elevated temperatures. Conversely, C-H bending vibrations (890–725 cm^{-1}) were more distinct in SP800, indicating the formation of thermally stable aromatic structures [37].

The morphological structure of the biochars was examined by FESEM (Fig. 2). FESEM images revealed a rough surface with grooves and small, uniformly distributed pores in SP600 (Fig. 2(a)). In contrast, SP800 (Fig. 2(b)) exhibited a more brittle surface, characterized by layered fractures and larger, more prominent pores. These differences in surface morphology reflect the influence of high-temperature pyrolysis, which promotes the decomposition of major organic components in the SP structure, including cellulose, hemicellulose, and lignin. This observation is consistent with the increasing specific surface area observed in SP800. Moreover, EDS analysis demonstrated that the SP800 exhibited the highest Carbon (C) content significantly. This increase reflects the development of more stable carbon structures with a tendency toward ordered aromatic structures, characteristic of high-temperature pyrolysis processes [38]. In contrast, the Oxygen (O) content decreased from 11.9 wt% in SP600 to 8.6 wt% in SP800, consistent with the FT-IR spectra (Fig. 1) which showed a decrease in the peak intensity corresponding to oxygen-containing functional groups (e.g., Hydroxyl (-OH), Carboxyl (C=O), and ester groups) due to

their decomposition during high pyrolysis temperature.

B. Lead Adsorption Performance

The lead adsorption performance of the biochar was evaluated by lead removal efficiency and lead adsorption capacity, as demonstrated in Table 2. The results revealed that SP800 exhibited a lead removal efficiency of 99.84 ± 0.05% and an adsorption capacity of 29.95 ± 0.07 mg/g, both of which were significantly higher than those observed for SP600. This enhancement is mainly attributed to the structural development of the biochar at higher pyrolysis temperatures, including increased specific surface area and the formation of a porous network suitable for lead adsorption [39]. The higher temperature promoted the decomposition of organic components during pyrolysis, which contributed to the development of micropores and mesopores, thereby increasing the available surface area for interactions with heavy metal ions [40]. Furthermore, the formation of a well-developed porous structure facilitated the diffusion of metal ions into the internal framework of the biochar, leading to improved adsorption performance. In addition, the increase in EC observed in SP800 also indicated a more negative zeta potential (ζ-potential) [31], which strengthened electrostatic attraction between Pb^{2+} ions and the biochar surface [41]. This mechanism was further supported by structural changes in the carbon matrix, including greater sp^2 carbon formation, graphitization, and continuous electron pathways, all of which enhanced electron mobility and supported electrostatic adsorption mechanisms [32]. Moreover, the FT-IR analysis in Fig. 1 supported these findings by showing that SP800 led to an obvious reduction in oxygen-containing functional groups (including hydroxyl (-OH), carbonyl (C=O), and alcohol/ester (C-O) groups) compared to SP600. Specifically, significant decreases in -OH (3770-3720 cm^{-1}) and C=O (1780–1700 cm^{-1}) were observed in SP800, contributing to the increased alkalinity of the biochar surface and enhancing its affinity for heavy metal ion binding. The reduction of these functional groups further indicated structural rearrangements in the carbon framework, which improved adsorption performance via ion exchange and complexation mechanisms [42]. These findings are consistent with a previous study by Escudero-Curiel et al. [43], which indicates that biochars produced at higher pyrolysis temperatures exhibited improved heavy metal removal performance due to the development of porous structures and favorable surface functionalities for adsorption processes.

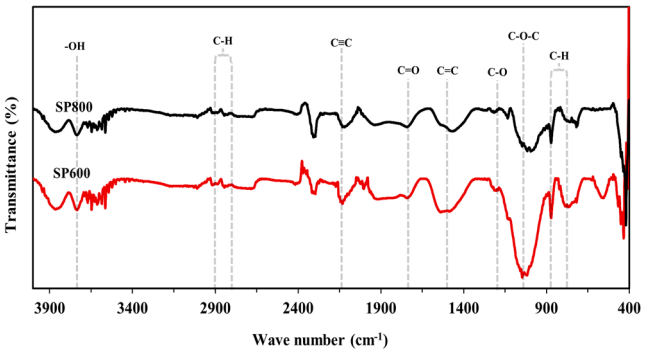

Fig. 1. FT-IR patterns of biochars obtained at different temperatures before lead adsorption.

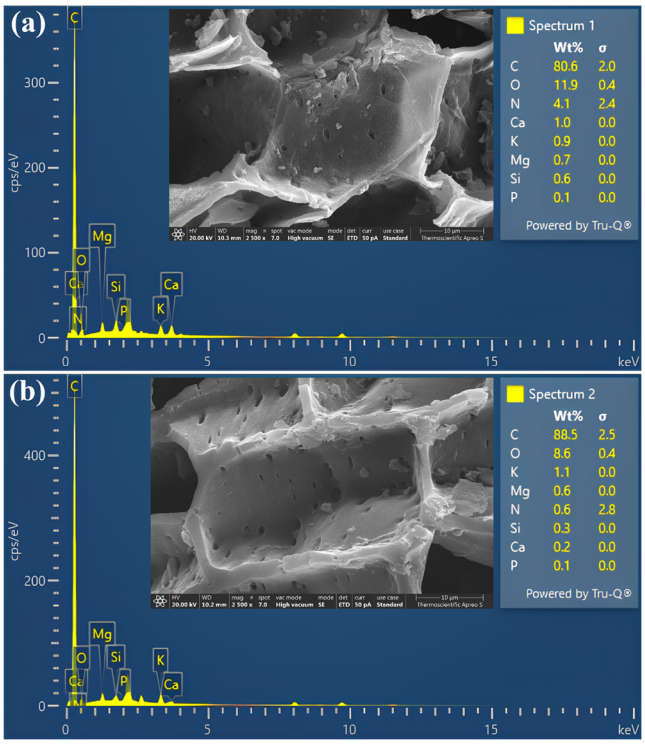

Fig. 2. FESEM-EDS analysis of biochars obtained at different temperatures before lead adsorption: (a) biochar produced at 600 °C, and (b) biochar produced at 800 °C.

C. Influence of Regenerating Solutions on Lead Adsorption Capacity

1) Lead desorption efficiency of regenerating solutions

The lead desorption efficiency of SP600 and SP800 was investigated using hydrochloric acid (HCl) and sodium nitrate ($NaNO_3$) solutions at concentrations of 0.1, 0.05, and 0.01 M, as presented in Fig. 3(a). The results revealed that SP600 exhibited higher lead desorption efficiency than SP800 across all concentrations of both HCl and $NaNO_3$. This difference is primarily attributed to the higher concentration of oxygen-containing functional groups in SP600, which are more likely to form bonds with Pb^{2+} that are easily disrupted during regeneration [44]. Additionally, variations in the EC between SP600 and SP800 also affected the lead desorption mechanism. The lower EC of SP600 suggests that its carbon structure was less graphitized and still contained abundant -OH and -COOH groups, which interact with Pb^{2+} ions primarily through ion-exchange mechanisms, allowing easier release upon regeneration. In contrast, SP800 exhibited a higher EC, indicating the formation of a more continuous sp^2 carbon network and a more negative ζ-potential [31]. As a result, Pb^{2+} ions were strongly bound to the biochar surface via electrostatic attraction and inner-sphere complexation, making desorption more difficult [32, 33]. Among the regenerating solutions examined, HCl demonstrated the highest desorption efficiency, particularly at a concentration of 0.1 M. This highlights the critical role of solution chemistry in lead desorption, as HCl, a strong acid, provides a high concentration of H^+ ions, significantly lowering the pH of the solution. The abundance of H^+ facilitates the displacement of Pb^{2+} from the biochar surface through on-exchange reactions. Additionally, Cl^- ions form soluble complexes with Pb^{2+}, such as $PbCl_2$, thereby enhancing the

lead desorption efficiency [45]. In contrast, $NaNO_3$ exhibited the lowest desorption efficiency. As a neutral salt, its inability to release H^+ ions limits its ability to disrupt Pb^{2+} functional group interactions on the biochar surface. Furthermore, Na^+ ions released from $NaNO_3$ are relatively large and ineffective at replacing Pb^{2+} during ion-exchange processes, further reducing the efficiency of lead desorption.

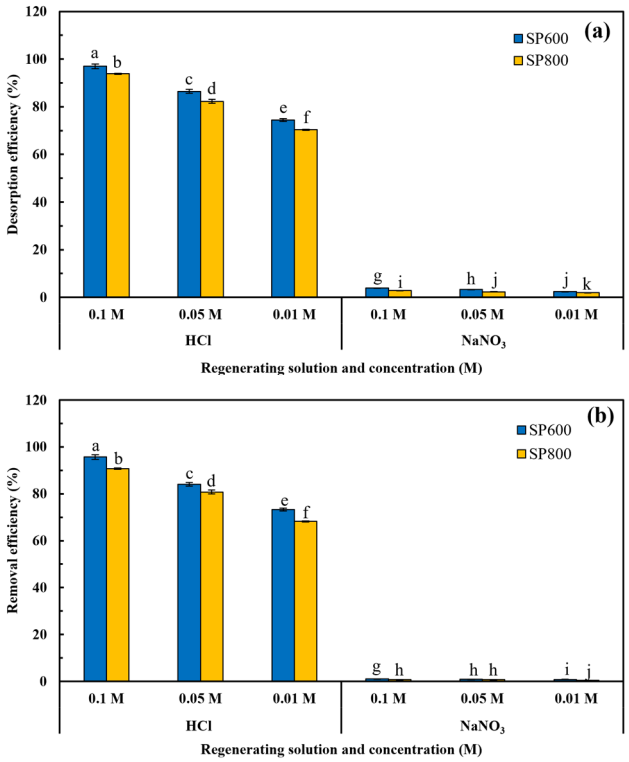

[a-k]Means with different superscripts are significantly different ($p < 0.05$)

Fig. 3. Effect of types and concentrations of regeneration solutions on lead adsorption capacity: (a) Desorption efficiency after regenerating, and (b) Removal efficiency after regenerating.

2) *Removal efficiency of regenerating solutions*

The lead removal efficiency of regenerated SP600 and SP800 was evaluated (Fig. 3(b)). Biochars regenerated with HCl exhibited the highest lead removal efficiency across all concentrations, particularly at 0.1 M. This is primarily attributed to HCl being a strong acid capable of releasing large amounts of H^+ ions, which promote the ion-exchange process with adsorbed Pb^{2+} ions. Moreover, Cl^- ions form soluble complexes with Pb^{2+}, such as $PbCl_2$, thereby enhancing lead desorption and promoting the regeneration of adsorption sites for reuse in subsequent cycles [45]. This finding is consistent with the lead desorption trends presented in Fig. 3(a). In contrast, $NaNO_3$ exhibited the lowest lead removal efficiency across all concentrations due to its neutral salt and inability to release H^+ ions. Consequently, previously adsorbed Pb^{2+} ions remained strongly bound to the biochar surface, resulting in poor surface regeneration and lower subsequent lead removal efficiency. SP600 consistently demonstrated higher lead removal efficiency after regeneration than SP800, which aligns with its higher lead desorption efficiency. This is attributed to the higher content of oxygen-containing functional groups, such as -OH and C=O, in SP600, which facilitates the release of Pb^{2+} ions and promotes more effective regeneration of the adsorption surface. Conversely, SP800, characterized by its finer pore structure and lower functional group content due to high pyrolysis temperatures, exhibited reduced regeneration efficiency [44]. Although SP800 showed a higher EC that initially enhanced electrostatic attraction toward Pb^{2+} ions, the formation of a continuous sp^2 carbon network and a more negative ζ potential led to the formation of inner-sphere complexes, thereby hindering the desorption of Pb^{2+} ions during regeneration [32]. Conversely, the lower EC of SP600 indicated a less graphitized carbon structure with a greater abundance of -OH and C=O functional groups, allowing Pb^{2+} ions to be released more easily, thereby improving surface regeneration and enhancing lead removal efficiency in subsequent cycles. [33]. These findings indicate that SP600 regenerated with 0.1 M HCl is a promising candidate for further investigation in multi-cycle adsorption-regeneration applications. Conversely, SP800 is more suitable for applications that require high lead removal efficiency in single-use adsorption processes.

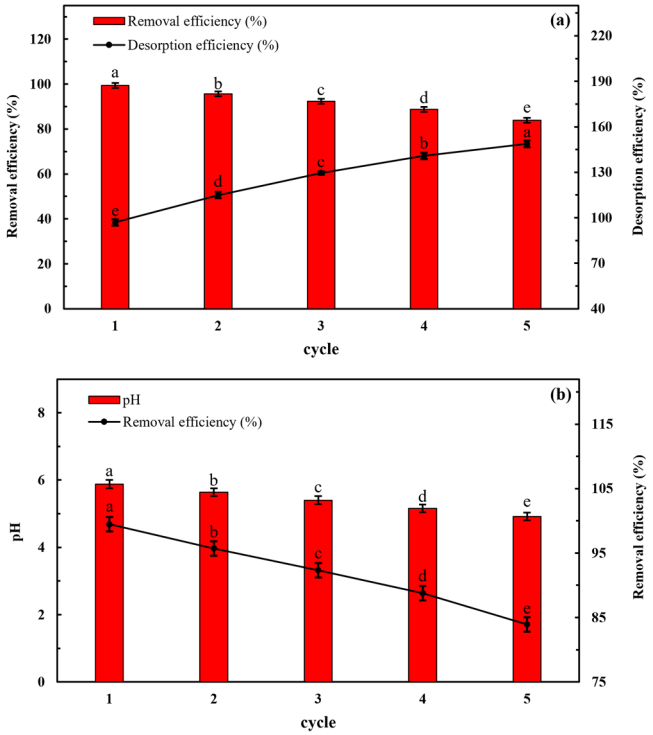

[a-e]Means with different superscripts are significantly different ($p < 0.05$)

Fig. 4. Regeneration capability of hydrochloric acid solution (HCl) with 0.1 M: (a) Removal efficiency and desorption efficiency of HCl 0.1 M, and (b) pH and removal efficiency of HCl 0.1 M.

3) *Regeneration capability of hydrochloric acid solution (HCl) on lead adsorption capability*

The regeneration capability of SP600 was further evaluated over five consecutive adsorption-regeneration cycles using 0.1 M HCl (Fig. 4(a)). The results represented a gradual decline in lead removal efficiency over successive cycles, decreasing from 99.47 ± 0.11% to 83.91 ± 0.10% by the fifth cycle. This progressive decline in adsorption performance is primarily attributed to pore blockage caused by residual compounds, such as $PbCl_2$, which accumulate within the biochar structure during the adsorption-regeneration process [46]. Furthermore, this reduction is also related to structural changes in the carbon matrix and the

gradual loss of surface functional groups (-OH, C=O, and C-O) is responsible for metal ion binding. Repeated exposure to acidic conditions during regeneration also contributed to surface degradation due to acid corrosion [47]. Conversely, the lead desorption efficiency progressively increased over successive cycles, from 97.01 ± 0.10% in the first cycle to 148 ± 0.13% in the fifth cycle. This increase is primarily due to ion-exchange processes between H^+ ions from HCl and adsorbed Pb^{2+} ions on the biochar surface [45]. Furthermore, Cl^- ions facilitated desorption by forming soluble complexes with Pb^{2+}, such as $PbCl_2$, thereby enhancing desorption efficiency over repeated regeneration cycles. This increase observed in the later cycles (exceeding 100%) is primarily attributed to the residual accumulation of Pb^{2+} ions from previous adsorption cycles. Their gradual accumulation and enhanced release during subsequent regeneration resulted in desorption efficiencies exceeding expected values under normal single-cycle conditions. Although lead desorption efficiency increased with repeated regeneration, the concurrent decline in lead removal efficiency highlights the limitations of multiple-use regeneration, particularly when using aggressive reagents like HCl. The progressive loss of functional groups essential for metal adsorption significantly compromises the long-term adsorption performance of the biochar. Although HCl effectively facilitates lead desorption, its detrimental effect on the surface structure and functional group (e.g., -OH, -COOH) must be carefully considered, especially for long-term applications.

D. Characteristics of Biochar after Lead Adsorption and Regeneration with HCl

The FT-IR analysis (Fig. 5) investigated the changes in surface functional groups of the fresh SP600, the biochar after lead adsorption (SP600Pb), and biochar after five consecutive adsorption-regeneration cycles (SP600RPb). A pronounced decrease in the peak intensity at 3770 cm^{-1} in SP600RPb indicates the loss of hydroxyl groups (-OH) due to acid corrosion from repeated HCl regeneration, which corresponds with the decline in lead removal efficiency (Fig. 4(a)). The peak intensity of the C-H stretching vibration (2960–2820 cm^{-1}) decreased in both SP600Pb and SP600RPb, indicating the decomposition or leaching of organic components during adsorption and regeneration cycles, further reducing lead adsorption capacity [48, 49]. The peak intensity at 1750 cm^{-1} (C=O stretching) significantly decreased in B600RPb, indicating the leaching of carbonyl groups after five consecutive cycles, which corresponds with the decline in lead adsorption capacity. The peak intensity of the C-H bending vibration at 1400 cm^{-1} showed a significant reduction in SP600Pb and a slight change in SP600RPb, reflecting the interaction between organic components, Pb^{2+}, and HCl used in the regeneration process. The peak intensity of the C-O-C stretching vibration at 1025 cm^{-1} decreased notably in SP600RPb. These functional groups play a crucial role in ion exchange and Pb^{2+} binding; their degradation affects the successive adsorption efficiency. Furthermore, the peak intensity at 890–725 cm^{-1}, associated with C-H bending, was significantly reduced in SP600RPb, suggesting the removal of organic matter from the biochar surface after five consecutive adsorption-regeneration cycles. Functional groups of this intensity may indirectly influence the interaction of the biochar surface with metal ions [37]. The peak intensity of Pb-O stretching at 560 cm^{-1} increased significantly in B600Pb, indicating the adsorption of Pb^{2+} ions onto the biochar surface. Conversely, the intensity of this peak decreased in SP600RPb, confirming the desorption of Pb^{2+} ions. These findings are consistent with the declining adsorption efficiency observed in Fig. 4(a) [48].

pH of the SP600RPb was analyzed to evaluate the effect of pH on lead removal efficiency, as presented in Fig. 4(b). The results demonstrated that the pH of SP600RPb gradually decreased with increasing regeneration cycles, from 5.88 ± 0.03 in the first cycle to 4.92 ± 0.02 in the fifth cycle. This trend corresponded to the observed decline in lead removal efficiency, reflecting the progressive degradation of the biochar structure due to the corrosive effect of HCl. Moreover, the decrease in pH significantly affected the adsorption process, as lead adsorption is generally most effective at near-neutral pH (~7). Under these conditions, SP600RPb effectively forms coordination bonds and participates in ion-exchange reactions with Pb^{2+} ions. However, as pH decreased due to repeated HCl regeneration, the increasing concentration of H^+ ions on the biochar surface led to direct competition with Pb^{2+} for active binding sites, such as -OH and C=O. As a result, the lead adsorption capacity declined significantly. Additionally, a consistently lower pH may also indicate the progressive loss of key oxygen-containing functional groups, such as -OH and C=O, which play critical roles in metal ion adsorption [50].

FESEM analysis examined the morphological structure of the SP600Pb and SP600RPb. The FESEM image of SP600Pb (Fig. 6(a)) exhibited significant surface changes, with numerous small particles distributed across the surface, which correspond to crystalline lead compounds adsorbed onto the biochar structure, indicating its effective adsorption capacity for Pb^{2+} ions. In contrast, the surface of SP600RPb (Fig. 6(b)) appeared rougher, with visible signs of surface corrosion and residual particles still observed, likely representing Pb^{2+} ions that remained after regeneration. These observations confirm that HCl is effective in desorbing Pb^{2+} ions, although small amounts of residual lead may remain. Furthermore, EDS analysis demonstrated that the lead content in SP800 decreased to 0.4 wt%, indicating partial desorption of lead from the biochar. However, decreases in both carbon and calcium contents were also observed. This suggests that, along with lead removal, essential structural components of the biochar, including functional groups involved in Pb^{2+} binding, may have been partially leached during the regeneration process.

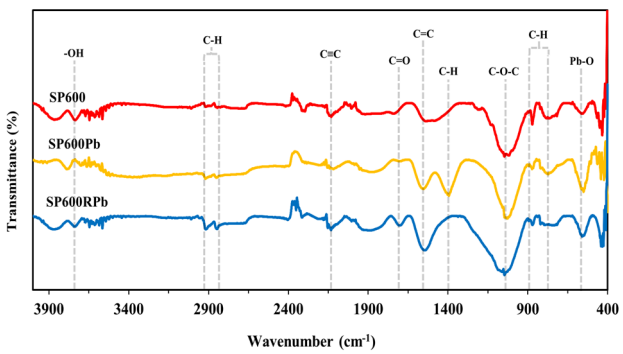

Fig. 5. FT-IR patterns of biochars obtained at 600 °C after lead adsorption and regeneration with HCl 0.1 M.

Table 3. Total production cost comparison of SP600Pb and SP600RPb

Category	SP600Pb		SP600RPb	
	Description	Cost (THB)	Description	Cost (THB)
Materials and chemicals				
Salak Peels	0.1 kg × 0 THB/kg	0	0.1 kg × 0 THB/kg	0
Nitrogen gas	6 L × 62.5 THB/L	375	6 L × 62.5 THB/L	375
DI water	0.75 L × 25 THB/L	18.75	1.25 L × 25 THB/L	31.25
Hydrochloric acid	-		0.5 L × 172 THB/L	86.00
Energy cost				
Drying (Hot air oven)	48 h × 1.2 kW × 4 THB/kWh	230.4	168 h × 1.2 kW × 4 THB/kWh	806.40
Pyrolysis (Electric furnace)	3 h × 2.5 kW × 4 THB/kWh	30	3 h × 2.5 kW × 4 THB/kWh	30
Biochar washing (Hot plate stirrer)	15 min × 0.5 kW × 4 THB/kWh	0.5	15 h 15 min × 0.5 kW × 4 THB/kWh	30.30
Lead adsorption (shaker)	24 h × 0.66 kW × 4 THB/kWh	63.36	120 h × 0.66 kW × 4 THB/kWh	316.80
Regeneration (shaker)	-		15 h × 0.66 kW × 4 THB/kWh	39.60
Biochar washing (Vacuum pump)	6 min × 0.1 kW × 4 THB/kWh	0.04	15 min × 0.1 kW × 4 THB/kWh	0.10
Filter biochar (Vacuum pump)	3 min × 0.1 kW × 4 THB/kWh	0.02	30 min × 0.1 kW × 4 THB/kWh	0.20
Total production cost (5 Cycle)		3590.35		1715.65

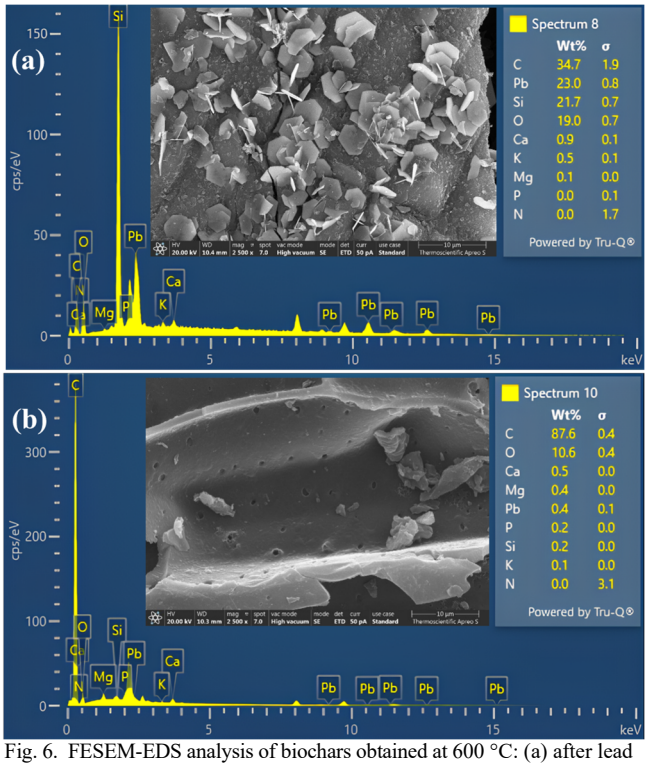

Fig. 6. FESEM-EDS analysis of biochars obtained at 600 °C: (a) after lead adsorption, and (b) after regeneration with HCl 0.1 M.

Table 4. Average costs per cycle comparison of SP600Pb and SP600RPb

Sample	Cycle	Total production cost (THB)	Average cost per cycle (THB/Cycle)
SP600Pb	5	3590.35	718.07
SP600RPb	5	1715.65	343.13

E. Cost Comparison Table for SP600Pb and SP600RPb

The total production costs of SP600Pb and SP600RPb were analyzed to evaluate the cost-effectiveness of biochar regeneration, as presented in Table 3. The results indicated that SP600RPb exhibited substantially lower total production costs and average costs per cycle compared to SP600Pb (Table 4). These findings highlight the potential of regeneration as an effective strategy for reducing production costs through more efficient resource application. While regeneration significantly reduced costs, the observed decline in lead removal efficiency with repeated cycles must be considered. Therefore, both economic and material performance should be considered to determine the optimal number of regeneration cycles and cost-effectiveness in practical applications. This study contributes to the SDGs [9, 10], particularly SDG 6 (Clean Water and Sanitation) and SDG 12 (Responsible Consumption and Production), by promoting the circular valorization of agricultural waste into functional biochar adsorbents. The ability to regenerate and reuse the biochar makes the adsorption process more sustainable and cost-effective compared to traditional coagulation–flocculation techniques, which generate secondary pollution [11].

V. Conclusion

This research demonstrated the significant influence of pyrolysis temperature on the lead removal efficiency and adsorption capacity of biochar derived from salak peels. Higher pyrolysis temperatures enhanced the physico chemical characteristics of the biochar, including specific surface area, pore size distribution, pore volume, electrical conductivity, and functional groups. Biochar produced at 800 °C (SP800Pb) exhibited superior lead removal efficiency and adsorption capacity during its initial application, indicating its suitability for single-use scenarios that require maximum adsorption performance. The effects of solution type and concentration were evaluated using Hydrochloric Acid (HCl) and Sodium Nitrate ($NaNO_3$) at concentrations of 0.1, 0.05, and 0.01 M. The findings revealed that biochar produced at 600 °C and regenerated with 0.1 M HCl (SP600RPb) exhibited superior lead desorption efficiency and removal efficiency, thereby representing the most promising condition for regeneration applications. After five adsorption–regeneration cycles with 0.1 M HCl, SP600RPb retained a lead removal efficiency of 83.91±0.10% and achieved a desorption efficiency of 148.73±0.13%. The desorption efficiency exceeding 100% was attributed to the gradual release of residual Pb^{2+} during subsequent regeneration cycles, indicating the enhanced ion-exchange behavior of the biochar. These results confirmed that 0.1 M HCl is an effective regenerant for extending the operational lifespan of biochar produced at 600 °C in heavy metal removal processes. Moreover, the utilization of salak peels,

an abundant agricultural by-product, as a feedstock for biochar production significantly reduces raw material costs. The use of a low-cost regenerant such as HCl offers substantial reductions in operational expenses associated with regeneration, particularly when compared to the repeated production of fresh biochar. In systems requiring multiple reuse cycles, this approach reduces the frequency of new biochar production, minimizes associated waste, and promotes resource efficiency.

Conflict of Interest

The authors declare no conflict of interest.

Author Contributions

Phruektinai Buakhiao conducted the experiments and wrote the manuscript; Thatchapol Chungcharoen designed the study and wrote the manuscript; Aud Jamkamon conducted the experiments and analyzed the data; Warunee Limmun analyzed the data and wrote the manuscript; Dithaporn Thungsotanon prepared tools for the experiments; all authors had approved the final version.

Acknowledgment

The authors would like to thank King Mongkut's Institute of Technology Ladkrabang for financially supporting this work [KREF016707].

References

[1] R. J. Moriarity, M. J. Wilton, L. J. Tsuji, A. Sarkar, and E. N. Liberda, "Evaluating human health risks from exposure to agricultural soil contaminants using one-and two-dimensional Monte Carlo simulations," *Environmental Research*, vol. 265, 120391, Jan. 2025.

[2] K. Raj and A. P. Das, "Lead pollution: Impact on environment and human health and approach for a sustainable solution," *Environ Chem Ecotoxicol,* vol. 5, pp. 79–85, Feb. 2023.

[3] Y. M. Bar-On and R. Milo, "The biomass distribution on earth," *Proceedings of the National Academy of Sciences,* pp. 6506–6511, vol. 115, May 2018.

[4] L. Hakim, R. Widyorini, W. D. Nugroho, and T. A. Prayitno, "Anatomical, chemical, and mechanical properties of fibrovascular bundles of Salacca (Snake Fruit) Frond," *Bioresources*, vol. 14, no. 4, pp. 7943–7957, Aug. 2019.

[5] T. Chungcharoen, W. Limmun, S. Srisang, K. Phetpan, N. Ruttanadech, P. Youryon, K. Pornprapa, and N. Srisang, "Enhanced biodiesel purification using coffee husk bioadsorbents: The role of pyrolysis temperature, KOH activation, and adsorption efficiency," *Renewable Energy*, vol. 244, 122700, May 2025.

[6] X. Zhang, B. Zhao, H. Liu, Y. Zhao, and L. Li, "Effects of pyrolysis temperature on biochar's characteristics and speciation and environmental risks of heavy metals in sewage sludge biochars," *Environmental Technology & Innovation*, vol. 26, 102288, 2022.

[7] M. Zhao, Y. Dai, M. Zhang, C. Feng, B. Qin, W. Zhang, N. Zhao, Y. Li, Z. Ni, Z. Xu, D. Tsang, and R. Qiu, "Mechanisms of Pb and/or Zn adsorption by different biochars: Biochar characteristics, stability, and binding energies," *Science of the Total Environment*, vol. 717, 136894, May 2020.

[8] X. F. Tan, S. B. Liu, Y. G. Liu, Y. L. Gu, G. M. Zeng, X. J. Hu, and L. H. Jiang, "Biochar as potential sustainable precursors for activated carbon production: Multiple applications in environmental protection and energy storage," *Bioresource Technology*, vol. 227, pp. 359–372, 2017.

[9] S. Meftah, K. Meftah, M. Drissi, I. Radah, K. Malous, A. Amahrous, and L. Bouyazza, "Heavy metal polluted water: Effects and sustainable treatment solutions using bio-adsorbents aligned with the SDGs," *Discover Sustainability*, vol. 6, no. 1, p. 137, 2025.

[10] K. Meftah, S. Meftah, H. Lamkhanter, T. Bouzid, Y. Rezzak, S. Touil, and A. Abid, "Extraction and optimization of *Austrocylindropuntia subulata* powder as a novel green coagulant," *Desalination and Water Treatment*, vol. 318, 100339, 2024.

[11] S. Zeng and E. Kan, "Adsorption and regeneration on iron-activated biochar for removal of microcystin-LR," *Chemosphere*, vol. 273, 129649, 2021.

[12] S. Sireeshaa, S. S. Kollurua, S. Agarwal, I. Sreedhar, and S. R. Kale, "Heavy metal removal from wastewater using nanomaterials—process and engineering aspects," *Process Safety and Environmental Protection*, vol. 150, pp. 323–355, June 2021.

[13] J. Bayuo, M. J. Rwiza, J. W. Choi, K. M. Mtei, A. Hosseini-Bandegharaei, and M. Sillanpää, "Adsorption and desorption processes of toxic heavy metals, regeneration and reusability of spent adsorbents: economic and environmental sustainability approach," *Advances in Colloid and Interface Science*, vol. 329, 103196, July 2024.

[14] Z. Liu and F. S. Zhang, "Removal of lead from water using biochars prepared from hydrothermal liquefaction of biomass," *Journal of Hazardous Materials*, vol. 167, no. 1–3, pp. 933–939, Sep. 2009.

[15] X. J. Tong, J. Y. Li, J. H. Yuan, and R. K. Xu, "Adsorption of Cu(II) by biochars generated from three crop straws," *Chemical Engineering Journal*, vol. 172, no. 2–3, pp. 828–834, Oct 2011.

[16] D. Kołodyńska, R. Wnętrzak, J. J. Leahy, M. H. B. Hayes, W. Kwapiński, and Z. Hubicki, "Kinetic and adsorptive characterization of biochar in metal ions removal," *Chemical Engineering Journal*, vol. 197, pp. 295–305, Dec. 2012.

[17] J. H. Park, Y. S. Ok, S. H. Kim, J. S. Cho, J. S. Heo, R. D. Delaune, and D. C. Seo, "Competitive adsorption of heavy metals onto sesame straw biochar in aqueous solutions," *Chemosphere*, vol. 142, pp. 77–83, Feb. 2016.

[18] W. Q. Zuo, C. Chen, H. J. Cui, and M. L. Fu, "Enhanced removal of Cd(II) from aqueous solution using $CaCO_3$ nanoparticle modified sewage sludge biochar," *RSC Advances*, vol. 7, no. 26, pp. 16238–16243, Mar 2017.

[19] Z. Mahdi, A. El Hanandeh, and Q. J. Yu, "Preparation, characterization and application of surface modified biochar from date seed for improved lead, copper, and nickel removal from aqueous solutions," *Journal of Environmental Chemical Engineering*, vol. 7, no. 5, 103379, Oct. 2019.

[20] J. Wu, T. Wang, J. Wang, Y. Zhang, and W. P. Pan, "A novel modified method for the efficient removal of Pb and Cd from wastewater by biochar: Enhanced the ion exchange and precipitation capacity," *Science of the Total Environment*, vol. 754, 142150, Apr. 2021.

[21] W. Ahmed, S. Mehmood, A. Núñez-Delgado, S. Ali, M. Qaswar, A. Shakoor, *et al*., "Enhanced adsorption of aqueous Pb (II) by modified biochar produced through pyrolysis of watermelon seeds," *Science of The Total Environment*, vol. 784, 147136, Oct. 2021.

[22] S. Sireesha, U. Upadhyay, and I. Sreedhar, "Comparative studies of heavy metal removal from aqueous solution using novel biomass and biochar-based adsorbents: characterization, process optimization, and regeneration," *Biomass Conversion and Biorefinery*, pp. 1–13, Jan. 2022.

[23] M. Tokarčíková, P. Peikertová, K. Č. Barabaszová, O. Životský, R. Gabor, and J. Seidlerová, "Regeneration possibilities and application of magnetically modified biochar for heavy metals elimination in real conditions," *Water Resources and Industry*, vol. 30, 100219, May 2023.

[24] K. S. Sopanrao, S. Gupta, S. Sireesha, U. Upadhyay, and I. Sreedhar, "Enhanced removal of Cu (II) and Ni (II) using MnOx-modified non-edible biochar: synthesis, characterization, optimization, thermo-kinetics, and regeneration," *Biomass Conversion and Biorefinery*, vol. 14, no. 18, pp. 21939–21961, Jun. 2024.

[25] A. Tomczyk, Z. Sokołowska, and P. Boguta, "Biochar physico-chemical properties: Pyrolysis temperature and feedstock kind effects," *Reviews in Environmental Science and Bio/Technology*, vol. 19, pp. 191–215, Feb. 2020.

[26] J. Smith, A. Doe, and K. Brown, "The impact of biochar on soil microbial communities: A meta-analysis," *Plant, Soil and Environment*, vol. 69, no. 2, pp. 125–135, Dec. 2023.

[27] S. Cheng, Y. Liu, B. Xing, X. Qin, C. Zhang, and H. Xia, "Lead and cadmium clean removal from wastewater by sustainable biochar derived from poplar saw dust," *Journal of Cleaner Production*, vol. 314, 128074, Feb. 2021.

[28] S. Katuwal, A. Ashworth, N. A. S. Rafsan, and P. Kolar, "Characterization of poultry litter biochar and activated biochar as a soil amendment for valorization," *Biomass*, vol. 2, no. 4, pp. 209–223, 2022.

[29] X. Xiao, Z. Chen, and B. H. Chen, "Atomic ratio as a smart linkage between pyrolytic temperatures, aromatic clusters and sorption properties of biochars derived from diverse precursory materials," *Scientific Reports*, vol. 6, 22644, Mar. 2016.

[30] L. Gao, Z. Li, W. Yi, Y. Li, P. Zhang, A. Zhang, and L. Wang, "Impacts of pyrolysis temperature on lead adsorption by cotton stalk-derived biochar and related mechanisms," *Journal of Environmental Chemical Engineering*, vol. 9, no. 4, 105602, Aug. 2021.

[31] S. R. Kane, R. Tiwari, and D. M. Mahapatra, "Physical and chemical mechanisms that influence the electrical conductivity of lignin-derived biochar," *Bioresource Technology*, vol. 342, 125944, Nov. 2021.
[32] R. S. Gabhi, D. W. Kirk, and C. Q. Jia, "Electrical conductivity of wood biochar monoliths and its dependence on pyrolysis temperature," *Carbon*, vol. 156, pp. 385–393, Sep. 2020.
[33] M. J. Bardi, J. M. Mutunga, and H. Ndiritu, "Effect of pyrolysis temperature on the physiochemical properties of biochar and its potential use in anaerobic digestion: A critical review," *Environmental Technology & Innovation*, vol. 32, 103349, Jul. 2023.
[34] R. Shan, Y. Shi, J. Gu, Y. Wang, and H. Yuan, "Single and competitive adsorption affinity of heavy metals toward peanut shell-derived biochar and its mechanisms in aqueous systems," *Chinese Journal of Chemical Engineering*, vol. 28, no. 5, pp. 1375–1383, May 2020.
[35] M. W. Yap, N. M. Mubarak, J. N. Sahu, and E. C. Abdullah, "Microwave induced synthesis of magnetic biochar from agricultural biomass for removal of lead and cadmium from wastewater," *Journal of Industrial and Engineering Chemistry*, vol. 45, pp. 287–295, Sep. 2017.
[36] A. Elnour, Y. Li, H. Zhang, M. Xu, and H. Zhang, "Effect of pyrolysis temperature on biochar microstructural evolution, physicochemical characteristics, and its influence on biochar/polypropylene composites," *Applied Sciences*, vol. 9, no. 6, p. 1149, Jun. 2019.
[37] S. Saleh, K. B. Kamarudin, W. A. W. A. K. Ghani, and L. S. Kheang, "Removal of organic contaminant from aqueous solution using magnetic biochar," *Procedia Engineering*, vol. 148, pp. 228–235, 2016.
[38] M. Keiluweit, P. S. Nico, M. G. Johnson, and M. Kleber, "Dynamic molecular structure of plant biomass-derived black carbon (biochar)," *Environmental Science & Technology*, vol. 44, no. 4, pp. 1247–1253, Feb. 2010.
[39] J. Zhang, S. Chen, J. Huang, X. Hu, and C. Zhu, "Effect of deashing on activation process and lead adsorption capacities of sludge-based biochar," *Science of the Total Environment*, vol. 716, 137016, Jul. 2020.
[40] T. M. A. Babeker and Q. Chen, "Heavy metal removal from wastewater by adsorption with hydrochar derived from biomass: current applications and research trends," *Current Pollution Reports*, vol. 7, pp. 54–71, Mar. 2021.
[41] X. Yang, J. Yang, Y. Jiang, L. Wei, and X. Huang, "Surface functional groups of carbon-based adsorbents and their roles in the removal of heavy metals from aqueous solutions: a critical review," *Chemical Engineering Journal*, vol. 366, pp. 608–621, May 2019.
[42] S. Escudero-Curiel, V. Acevedo-García, M. Á. Sanromán, and M. Pazos, "Eco-approach for pharmaceutical removal: Thermochemical waste valorisation, biochar adsorption and electro-assisted regeneration," *Electrochimica Acta*, vol. 389, 138694, Feb. 2021.
[43] A. Herath, C. A. Layne, F. Perez, E. B. Hassan, C. U. Pittman Jr, and T. E. Mlsna, "KOH-activated high surface area Douglas Fir biochar for adsorbing aqueous Cr (VI), Pb (II) and Cd (II)," *Chemosphere*, vol. 269, 128409, Mar. 2021.
[44] J. Qu, L. Zhang, Y. Qiao, Y. Wang, and Q. Wang, "Microwave-assisted one pot synthesis of β-cyclodextrin modified biochar for concurrent removal of Pb (II) and bisphenol A in water," *Carbohydrate Polymers*, vol. 250, 117003, Jan. 2020.
[45] H. Zhang, X. Wang, Y. Chen, L. Zhou, and Y. Xu, "Influence of regeneration cycles on the pore structure and adsorption capacity of biochar for heavy metal removal," *Bioresource Technology*, vol. 192, pp. 283–291, May 2015.
[46] Y. Li, J. Liu, Y. Wang, Z. Lu, and C. Wu, "Structural damage and performance deterioration of biochar after repeated acid regeneration for heavy metal removal," *Environmental Pollution*, vol. 220, part B, pp. 1305–1313, Nov. 2017.
[47] J. H. Park, Y. S. Ok, S. H. Kim, J. S. Cho, J. S. Heo, R. D. Delaune, and D. C. Seo, "Cadmium adsorption characteristics of biochars derived using various pine tree residues and pyrolysis temperatures," *Journal of Colloid and Interface Science*, vol. 553, pp. 298–307, Feb. 2019.
[48] J. Coates, "Interpretation of infrared spectra, a practical approach," *Encyclopedia of Analytical Chemistry*, pp. 10815–10837, 2000.
[49] E. Smidt, K. U. Eckhardt, P. Lechner, H. R. Schulten, and P. Leinweber, "Characterization of different decomposition stages of biowaste using FT-IR spectroscopy and pyrolysis-field ionization mass spectrometry," *Biodegradation*, vol. 16, pp. 67–79, Feb. 2005.
[50] Y. Zhou, X. Sun, S. Zhang, and H. Wu, "Surface acidification of bamboo biochar during repeated adsorption–desorption of Cu(II) and its impact on adsorption performance," *Environmental Pollution*, vol. 223, pp. 71–79, Mar. 2017.